Horsch Hasse Shchekin Agarwal Eckelsbach Vrabec Müller Jackson

The excess equimolar radius of liquid drops

Martin Horsch* and Hans Hasse
Lehrstuhl für Thermodynamik, Fachbereich Maschinenbau und Verfahrenstechnik, Technische Universität Kaiserslautern, Erwin-Schrödinger-Str. 44, 67663 Kaiserslautern, Germany

Alexander K. Shchekin
Department of Statistical Physics, Faculty of Physics, Saint Petersburg State University, ul. Ulyanovskaya, Petrodvoretz, 198504 Saint Petersburg, Russia

Animesh Agarwal, Stefan Eckelsbach, and Jadran Vrabec
Lehrstuhl für Thermodynamik und Energietechnik, Institut für Verfahrenstechnik, Universität Paderborn, Warburger Str. 100, 33098 Paderborn, Germany

Erich A. Müller and George Jackson†
Department of Chemical Engineering, Centre for Process Systems Engineering, Imperial College London, London SW7 2AZ, United Kingdom

(Dated: 23rd September 2011)

The curvature dependence of the surface tension is related to the excess equimolar radius of liquid drops, i.e., the deviation of the equimolar radius from that defined with the macroscopic capillarity approximation. Based on the Tolman [J. Chem. Phys. **17**, 333 (1949)] approach and its interpretation by Nijmeijer *et al.* [J. Chem. Phys. **96**, 565 (1991)], the surface tension of spherical interfaces is analysed in terms of the pressure difference due to curvature. In the present study, the excess equimolar radius, which can be obtained directly from the density profile, is used instead of the Tolman length. Liquid drops of the truncated-shifted Lennard-Jones fluid are investigated by molecular dynamics simulation in the canonical ensemble, with equimolar radii ranging from 4 to 33 times the Lennard-Jones size parameter σ. In these simulations, the magnitudes of the excess equimolar radius and the Tolman length are shown to be smaller than $\sigma/2$. Other methodical approaches, from which mutually contradicting findings have been reported, are critically discussed, outlining possible sources of inaccuracy.

PACS numbers: 05.70.Np, 68.03.-g, 05.20.Jj, 68.03.Cd

I. INTRODUCTION

The macroscopic capillarity approximation consists in neglecting the curvature dependence of the surface tension γ of a spherical liquid drop. Accordingly, the surface tension of a curved interface in equilibrium is approximated by the value γ_0 in the zero-curvature limit, i.e., for a planar vapour-liquid interface. The Young-Laplace equation [1–3] for spherical interfaces relates the macroscopic surface tension to a characteristic radius R_κ of the liquid drop

$$\frac{\gamma_0}{R_\kappa} = \frac{1}{2}\left(p' - p''\right) = \varphi, \tag{1}$$

which will be referred to as the capillarity radius here. Both the factor $1/R_\kappa$ and the difference between the liquid pressure p' and the vapour pressure p'' characterize the extent by which the surface is curved; the notation $\varphi = (p' - p'')/2$ for half of the pressure difference is introduced for convenience. At equilibrium, the temperature is the same for both phases, and the pressures p' and p'' correspond to states with the same chemical potential. The surface tension γ_0 of the planar vapour-liquid phase boundary, which is relatively easy to access experimentally, couples these two measures of curvature as a proportionality constant.

In combination with an equation of state for the bulk fluid, microscopic properties such as the radius of a small liquid drop can thus be deduced from the macroscopic state of the surrounding vapour, i.e., from its supersaturation ratio, and vice versa. This approach is the most widespread interpretation of the Gibbs theory of interfaces [4, 5], and it is the point of departure for the classical nucleation theory (CNT) as introduced by Volmer and Weber [6] and further developed by Farkas [7] as well as subsequent authors [8–10]. With the Gibbs approach one presumes a sharp dividing surface between the phases, a conceptual picture that does not reflect the physical phenomena present at the molecular length scale. However, this abstraction is precisely its strength.

* Co-affiliated with Imperial College and Universität Paderborn
† Corresponding author: G. Jackson; g.jackson@imperial.ac.uk; http://www3.imperial.ac.uk/people/g.jackson

Instead of discussing thermodynamic properties such as the density, the pressure tensor and the free energy density in a localized way, interfacial excess quantities can be assigned to the formal dividing surface as a whole.

It should be recognized that significant size effects on interfacial properties had already been detected experimentally by Weber [11] at the turn of the last century. This was also known to Farkas [7] who stated explicitly that the capillarity approximation should be expected to fail for radii at the length scale of the intermolecular interactions. In the absence of a better approximation, however, the surface tension of the planar phase boundary had to be used for nucleation theory, and little has changed in this respect in the meantime.

In case of significant deviations from the macroscopic capillarity approximation, liquid drops cannot be characterized sufficiently by a single effective radius. Instead, the capillarity radius R_κ is distinct from the equimolar radius R_ρ, which is also known as the Gibbs adsorption radius. For a single-component system, the latter is defined by the zero excess density criterion

$$\int_0^{R_\rho} dz\, z^2\, [\rho(z) - \rho'(\mu, T)] + \int_{R_\rho}^{\infty} dz\, z^2\, [\rho(z) - \rho''(\mu, T)] = 0, \tag{2}$$

i.e., by comparing a step function based on the bulk liquid and vapour number densities $\rho'(\mu, T)$ and $\rho''(\mu, T)$ as functions of the chemical potential μ and the temperature T, respectively, with the microscopic radial density profile $\rho(z)$. By convention, the density ρ corresponds to the number of particles per volume here, rather than their mass, and z denotes the distance from the centre of mass of the liquid drop. In the following discussion, T is treated as a parameter (instead of a variable), so that total differentials are to be understood as partial differentials at constant temperature.

For curved interfaces in equilibrium, the chemical potential deviates from its saturated value μ_s for a flat interface. In case of a drop, both phases are supersaturated. To realize this, it is sufficient to consider the Gibbs-Duhem equation for a curved phase boundary

$$d\,(p' - p'') = (\rho' - \rho'')\, d\mu. \tag{3}$$

For a planar interface, both phases coexist at the saturation condition ($\mu = \mu_\mathrm{s}$) and the pressure difference is zero. Raising the value of the liquid pressure p' over the vapour pressure p'' therefore increases the chemical potential μ, which must be equal for both phases in (stable or unstable) equilibrium, so that its value for a system with a liquid drop will exceed μ_s. The precise conditions can be determined from the pressure difference between the fluid phases by means of an equation of state.

Beside R_κ and R_ρ, a thermodynamically relevant definition of the liquid drop size is given by the surface of tension radius

$$R_\gamma = \frac{\gamma}{\varphi}, \tag{4}$$

which is also known as the Laplace radius. It can be obtained by inserting the actual value of the surface tension γ of the system with the curved interface (not the planar limit value) into the Young-Laplace equation. This radius can be related to the surface area a and to the volume V of the drop

$$R_\gamma\, da = 2\, dV. \tag{5}$$

The excess grand potential Σ of the surface thus evaluates to

$$R_\gamma\, d\Sigma = 2\gamma\, dV, \tag{6}$$

in terms of the surface tension

$$\gamma = \frac{d\Sigma}{da}. \tag{7}$$

Modified versions of the Young-Laplace equation, which allow for the use of different radii in an analogous way, were introduced by Buff [12, 13] and Kondo [14].

The present study deals with the deviation between the capillarity radius R_κ, the equimolar radius R_ρ and the surface of tension radius R_γ of a liquid drop in equilibrium with a supersaturated vapour. As Tolman [15–17], following Gibbs, showed on the basis of axiomatic thermodynamics, one of these differences, now commonly referred to as the Tolman length

$$\delta = R_\rho - R_\gamma, \tag{8}$$

is sufficient to characterize the curvature dependence of the surface tension [17]

$$\frac{d \ln R_\gamma}{d \ln \gamma} = 1 + \frac{1}{2}\left(\frac{\delta}{R_\gamma} + \left[\frac{\delta}{R_\gamma}\right]^2 + \frac{1}{3}\left[\frac{\delta}{R_\gamma}\right]^3\right)^{-1}. \tag{9}$$

It is important to point out that this relation is exact, strictly following the approach of Gibbs, i.e., without neglecting any of the higher-order curvature terms. The cubic expression derives from an integral over the spherical density profile. However, Eq. (9) is often transformed into a polynomial expansion for γ_0/γ, which contains an infinite number of terms and has to be truncated, e.g., after the second-order contribution in terms of curvature [18]

$$\frac{\gamma_0}{\gamma} = 1 + \frac{2\delta_0}{R_\gamma} + 2\left(\frac{\lambda}{R_\gamma}\right)^2 + \mathcal{O}\big(R_\gamma^{-3}\big). \tag{10}$$

Here, δ_0 is the Tolman length in the zero-curvature (infinite radius) limit. Castellanos *et al.* [19] have conjectured that «the Tolman length is related to the interfacial width Δ^σ according to $\Delta^\sigma \approx 2\delta$.» The Block length λ, which characterizes the effect of Gaussian curvature that becomes predominant when δ is very small or for systems where, due to an inherent symmetry, $\delta = 0$ holds by construction, has recently been investigated by Block *et al.* [18]; a similar leading term, proportional to $R_\gamma^{-2} \ln R_\gamma$,

has also been deduced by Bieker and Dietrich [20] from DFT based on a Barker-Henderson perturbation expansion.

One should keep in mind that the Tolman equation as given by Eq. (9) is valid for curved phase boundaries of pure fluids in general, whereas truncated polynomial expansions in terms of the curvature $1/R_\gamma$ like Eq. (10) necessarily break down for liquid drops at the molecular length scale. In practice, one of the major problems of the Tolman approach is that it analyses the surface tension in terms of the radii R_ρ and R_γ. While R_ρ can be immediately obtained from the density profile, R_γ is by definition related to γ itself. Since for highly curved interfaces the value of γ is disputed or unknown [21, 22], the surface of tension radius R_γ is correspondingly uncertain.

To resolve this issue, we reformulate Tolman's theory in terms of R_κ and R_ρ. This leads to greater transparency, since the capillarity radius R_κ can be obtained on the basis of the surface tension in the planar limit γ_0, which is experimentally accessible, and properties of the (stable and metastable) bulk fluid. It is related to the pressure difference between the coexisting phases in equilibrium, which is a bulk property as well, since it can be determined from μ and T with an equation of state for the fluid. All information on the molecular structure of the curved interface can thus be captured by a single undisputed quantity here, namely the equimolar radius R_ρ.

For this approach, the excess equimolar radius, defined as

$$\eta = R_\rho - R_\kappa, \tag{11}$$

plays a role similar to the Tolman length, and the macroscopic quantity φ is used instead of $1/R_\gamma$ as a measure of the influence of curvature on the thermophysical properties of the interface and the bulk phases. In this way, the thermodynamics of liquid drops are discussed by following a new route that relies on the density profiles and bulk properties only, avoiding the intricacies of defining the pressure tensor or the change in the surface area as required by other approaches.

The present method is related to the «direct determination» of δ_0 proposed by Nijmeijer *et al.* [23], as recently applied by van Giessen and Blokhuis [24] on the basis of a representation of φR_ρ over $1/R_\rho$ with

$$-\delta_0 = \frac{1}{\gamma_0}\left(\lim_{R_\rho\to\infty}\frac{d}{d(1/R_\rho)}\varphi R_\rho\right), \tag{12}$$

as depicted in Fig. 1. However, the implementation suggested here is methodologically different from that of van Giessen and Blokhuis which relies on a pressure tensor to obtain φ, whereas in the present work, the pressure difference is determined by molecular dynamics (MD) simulation of the bulk fluids. Applying the definitions of the capillarity radius and the excess equimolar radius, Eq.

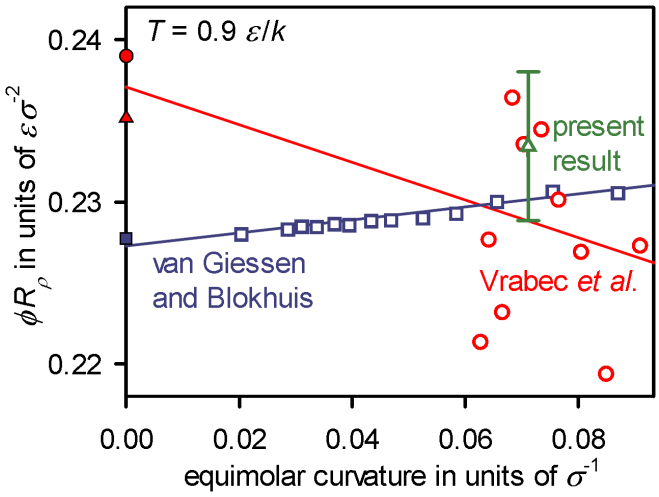

Figure 1. Representation of van Giessen and Blokhuis [24], showing φR_ρ as a function of the equimolar curvature $1/R_\rho$ for liquid drops of the truncated-shifted Lennard-Jones fluid at $T = 0.9\ \varepsilon/k$, where the equimolar radius R_ρ is determined from the density profiles and φ from the difference between the values of the normal component of the Irving-Kirkwood pressure tensor in the homogeneous regions inside the liquid drop as well as outside, i.e., in the homogeneous supersaturated vapour. In comparison with the results of van Giessen and Blokhuis (□), the data of Vrabec *et al.* [25] (○), which were obtained by the same method, are included here along with a data point (△) where φ is determined by MD simulation of the homogeneous fluid. The data for the planar surface tension γ_0 are taken from simulations of Vrabec *et al.* (●) and van Giessen and Blokhuis (■) as well as the correlation of Vrabec *et al.* (▲). The continuous lines are guides to the eye: In the planar limit, a positive slope corresponds to a negative Tolman length and vice versa, cf. Eq. (12).

(12) transforms to

$$-\delta_0 = \lim_{R_\rho\to\infty}\frac{d(R_\rho/R_\kappa)}{d(1/R_\rho)} = \lim_{R_\rho\to\infty}\frac{d(\eta/R_\kappa)}{d(1/R_\rho)}, \tag{13}$$

facilitating an analysis of interface properties in terms of the radii R_κ and R_ρ as well as the deviation η between them.

This article is structured as follows: In Section II, a review is made of the available routes to the Tolman length and the surface tension by molecular simulation. MD simulation methods immediately related to nucleation itself, from which information of the excess free energy of curved interfaces can also be deduced [26–29], are not included in that discussion; in this regard, the reader is referred to Chkonia *et al.* [30]. Section III is dedicated to a brief outline of how Tolman's thermodynamic approach can be transformed by analysing the surface tension in terms of η and φ rather than δ and $1/R_\gamma$. The methodology and the results of a series of canonical ensemble MD simulations, where the excess equimolar radius is obtained solely on the basis of density profiles, are presented in Section IV. An interpretation of these results is given

in Section V, placing the present findings in the context of the multitude of mutually contradicting hypotheses proposed in the literature.

II. THE TOLMAN LENGTH FROM MOLECULAR SIMULATION

A. Analysis of the planar interface

For the planar interface, the definition of the Tolman length given by Eq. (8) ceases to be applicable, as the surface of tension radius R_γ becomes ill-defined in the absence of curvature, since the pressure is equal on both sides of the interface in this case. Therefore, the planar interface Tolman length δ_0 necessarily has to be derived from considerations pertaining to curved geometries. It can be obtained either by extrapolating results for δ to the macroscopic limit $\varphi \to 0$ (i.e., $R_\gamma \to \infty$) or by constructing the limit explicitly from expressions for the radii R_ρ and R_γ. The latter approach was followed by Fisher and Wortis [31] who, on the basis of Landau (square-gradient) theory, derived the relation

$$-\delta_0 = \left(\int_{z=-\infty}^{z=\infty} d\rho_0(z) \frac{d\rho_0(z)}{dz}\right)^{-1} \int_{z=-\infty}^{z=\infty} d\rho_0(z) \frac{d\rho_0(z)}{d\ln z} + \frac{1}{\Delta\rho} \int_{z=-\infty}^{z=\infty} d\rho_0(z)\, z, \tag{14}$$

in terms of the density profile $\rho_0(z)$ of the planar interface. This expression can also be extended to account for the pair density profile, whereby Eq. (14) becomes a limiting case [32, 33].

The available computational methods for evaluating the Tolman length of curved interfaces, however, involve the determination of the surface tension γ. It is usually the methodology related to the evaluation of γ that is both the crucial and the most debatable step, which is made evident by the contradictory findings for γ (and consequently also for δ_0) obtained from different methods. Three routes to the surface tension of liquid drops will now be discussed briefly: the mechanical route as implemented by Thompson *et al.* [34], the grand canonical route of Schrader *et al.* [35] and the variational route developed by Sampayo *et al.* [22].

Many different versions and combinations of these approaches exist [36–38], but it would be inappropriate to attempt a full appreciation of the complete body of work here. The reader is directed to the excellent review by Henderson [39] for a detailed discussion of the underlying statistical mechanical approaches.

B. The mechanical route

The mechanical route to the surface tension is based on the Bakker-Buff equation for spherical interfaces [13, 34, 40, 41]

$$\gamma = R_\gamma^{-2} \int_{z=0}^{z=\infty} dz\, z^2 \left[p_\mathrm{n}(z) - p_\mathrm{t}(z)\right], \tag{15}$$

in terms of the normal component $p_\mathrm{n}(z)$ and the two (equal) tangential components $p_\mathrm{t}(z)$ of the diagonalized pressure tensor, which is considered as a spherical average, and where the integration is from the centre of the drop (z= 0). With this relation one expresses the work required for a reversible isothermal deformation of the system that leads to an infinitesimal increase of the surface area at constant volume, which coincides with the associated free energy difference. It is sufficient to compute either the normal or the tangential pressure profile, since both are related by [34, 42]

$$\frac{dp_\mathrm{n}}{d\ln z} = 2\left(p_\mathrm{t} - p_\mathrm{n}\right). \tag{16}$$

At mechanical equilibrium, Eq. (15) can thus be transformed to [34]

$$2\gamma^3 = -\varphi^2 \int_{z=0}^{z=\infty} dp_\mathrm{n}(z)\, z^3, \tag{17}$$

a term in which R_γ no longer appears. The surface of tension radius R_γ can be obtained from the Young-Laplace equation once the surface tension γ is known.

The most widespread implementation of this approach in terms of intermolecular pair potentials makes use of the Irving-Kirkwood (IK) [43] pressure tensor, which was first applied to (spherical) interfaces by Buff [13] and underlies the simulation studies of Vrabec *et al.* [25] as well as those of van Giessen and Blokhuis [24]. Its normal component is given by [34, 43]

$$p_\mathrm{n}(z) = kT\rho(z) + \sum_{\{i,j\}\in\mathbf{S}} -\frac{du_{ij}}{dr_{ij}} \frac{|\mathbf{z}\cdot\mathbf{r}_{ij}|}{4\pi z^3\, r_{ij}}, \tag{18}$$

wherein k is the Boltzmann constant and the summation covers the set $\mathbf{S}$ containing all sets of particles i and j that are connected by a line intersecting a sphere of radius z around the centre of mass. The intersection coordinates relative to the centre of mass of the liquid drop are represented by $\mathbf{z}$ and the distance between the particles by $\mathbf{r}_{ij}$ with $r_{ij} = |\mathbf{r}_{ij}|$, while $-du_{ij}/dr_{ij}$ is the force acting between the two particles i and j.

Regarding the mechanical route as described here, various issues arise:

- It is not clear to what extent the spherical average of the pressure tensor succeeds in accounting for the free energy contribution of capillary waves, i.e., the excited vibrational modi of the interface [44, 45].
- Irving and Kirkwood [43] originally proposed their expression for the special case of «a single component, single phase system». Its derivation relies on truncating an expansion in terms of derivatives of

the pair density $\rho^{(2)}$ after the first term, thereby disregarding the density gradient completely. For a liquid drop, this can lead to inaccuracies: «at a boundary or interface ... neglecting terms beyond the first may not be justified» [43].

- By construction, the mechanical route cannot be separated from the assumption of a mechanical equilibrium that underlies both the basic approach, i.e., Eqs. (15) to (16), and the derivation of the IK pressure tensor, cf. Eq. (18). For nanoscopic liquid drops, however, configurations deviating from the equilibrium shape correspond to a significant fraction of the partition function.

- The non-unique nature of the pressure tensor, which for a planar interface does not have a consequence on the computed value of the surface tension [46], leads to an inconsistent description for a curved interface [38, 39, 47]. However, the Harasima pressure tensor [41], where the set **S** is defined differently and the tangential pressure profile $p_\mathrm{t}(z)$ is computed instead of the normal component $p_\mathrm{n}(z)$, has been found to agree rather well with the IK tensor [25, 37, 46].

C. The grand canonical route

From an analysis of the canonical partition function and its dependence on the characteristic length L of otherwise similar systems, Binder [45] derived very useful scaling laws for the probability $\omega(\rho_\mathrm{min})$ of relatively small subvolume to have the density ρ_min corresponding to a maximum of the local free energy, i.e., the least probable local density between ρ' and ρ''. It follows that «the probability of a *homogeneous* state with order parameter ρ_min decreases exponentially fast with the volume» while for cases where the corresponding subvolume is situated within a phase boundary the probability «decreases exponentially fast with the interface area» [45]. The surface excess of the grand potential (per unit surface area) can thus be determined as

$$f^\mathrm{E} = \lim_{a\to\infty} \frac{\Sigma}{a} = kT \lim_{L\to\infty} \frac{\ln \omega(\rho_\mathrm{min})}{a(L)}, \qquad (19)$$

which is related to the surface tension by $\gamma = d\Sigma/da$. Therein, the term $a(L)$ describes the dependence of the surface area on the characteristic length of the system [45], e.g., $a(L) = 2L^2$ for a planar slab in a cubic volume $V = L^3$ with standard periodic boundary conditions.

Small subvolumes of a canonical system in the thermodynamic limit ($N \to \infty$) are equivalent to systems with constant μ, V and T so that grand canonical Monte Carlo (GCMC) simulation can equally be applied. Umbrella sampling may be used to fully sample the relevant range of values for the order parameter [48, 49], corresponding to the number of particles N present in the grand canonical system. Thereby, a profile is obtained for the free energy density $f(N)$ or $f(\rho)$, i.e., the dependence of the grand potential per volume unit on the order parameter.

To analyse liquid drops of a certain size, however, the limit $a \to \infty$ cannot be applied since the area a of the surface of tension is fixed. Instead, the surface excess term $f^\mathrm{E}(R_\rho)$ is determined from expressions based on the equimolar radius [35]

$$f(\rho) = \frac{V'}{V}\rho'(R_\rho)\mu(R_\rho) + \frac{V''}{V}\rho''(R_\rho)\mu(R_\rho) + \frac{4\pi R_\rho^2}{V} f^\mathrm{E}(R_\rho). \qquad (20)$$

$V' = 4\pi R_\rho^3/3$ is the volume associated with the liquid phase here, $V'' = V - V'$ is the remainder of the volume and $\rho'(R_\rho)$ as well as $\rho''(R_\rho)$ are bulk densities related to the liquid drop and the surrounding vapour. The chemical potential $\mu(R_\rho)$ is equal for the vapour and liquid regions, but different from both the saturated bulk value μ_s and the chemical potential μ used for the grand canonical simulation itself. This formalism has recently been employed by Schrader *et al.* [21, 35] as well as Block *et al.* [18], to examine the interfacial properties of drops, bubbles, and symmetric mixtures in great detail.

The original method of Binder [45] was developed for planar interfaces. In the case of systems with a spherical geometry, the following points should be kept in mind:

- Following the approach of Schrader *et al.* [35], the surface tension γ can be accessed only indirectly, e.g., from Eq. (6), based on the surface of tension radius R_γ which also has to be obtained in a circuitous manner. Thereby, care should be taken not to confuse f^E with γ, or R_ρ with R_γ.

- Since the infinite size limit, cf. Eq. (19), does not apply to nanoscopic liquid drops and the systems under consideration can be extremely small, it is not generally possible to neglect the contribution of homogeneous configurations to $f(\rho)$ [45].

- The assumption that $4\pi R_\rho^2$ is the surface area associated with the surface excess for the grand potential of the system, as in Eq. (20), essentially amounts to applying the macroscopic capillarity approximation. Such an approach may be justified under certain circumstances, but for investigations of the *deviation* from capillarity it is of limited use only.

Other umbrella sampling based methods [50, 51], which will not be discussed here in detail, are confronted with similar difficulties, in particular regarding the relation between the surface tension and the surface excess free energy.

D. The variational route

The variational route to the surface tension is based on Bennett's [52] general considerations of the molecular

simulation of free energies and entropic quantites. In the canonical ensemble, the free energy difference $\Delta A = A_1 - A_0$ between two states with equal N, V and T is given by the quotient of the respective canonical partition functions Z_0 and Z_1, which can be evaluated as averages in terms of internal energy differences [52]

$$\exp\left(\frac{\Delta A}{kT}\right) = \frac{Z_0}{Z_1} = \frac{\langle \min\left(1, \exp\left([E_1 - E_0]/[kT]\right)\right)\rangle_1}{\langle \min\left(1, \exp\left([E_0 - E_1]/[kT]\right)\right)\rangle_0}, \quad (21)$$

where the index of the angular brackets denotes the system over which an ensemble average is taken. Bennett proposed the determination of these energy differences from «separately-generated samples» [52] for E_0 and E_1. If the two systems differ in the area of a phase boundary, then the free energy difference can be related to the surface tension, assuming that all other deviations between the two states are accurately taken into account.

Gloor *et al.* [36] introduced a version of this approach where differences between the two states are obtained from a single simulation run for an unperturbed system with the partition function Z_0. Corresponding configurations of the second, perturbed system are generated by performing small affine transformations, keeping the volume and the number of particles in both phases constant. In the limit of an infinitesimal distortion of the system, Eq. (21) can be simplified as [36, 53]

$$\frac{\Delta A}{kT} = -\ln\left\langle \exp\left(\frac{-\Delta E}{kT}\right)\right\rangle_0, \quad (22)$$

where $\Delta E = E_1 - E_0$, as the probability distribution functions of the ensembles corresonding to the unperturbed and the perturbed system converge, so that a separate sampling is no longer required. A third-order expansion in the inverse temperature [53]

$$\frac{\Delta A}{kT} = \frac{\langle \Delta E\rangle}{kT} - \frac{\langle \Delta E^2\rangle - \langle \Delta E\rangle^2}{2(kT)^2} + \frac{\langle \Delta E^3\rangle - 3\langle \Delta E^2\rangle\langle \Delta E\rangle + 2\langle \Delta E\rangle^3}{6(kT)^3}, \quad (23)$$

can be used to increase the precision of the simulation results [22, 36]. The surface tension is then immediately obtained from $\Delta A/\Delta a$, since the distortion of the interface itself (as opposed to its increase in area) makes a negligible contribution to the free energy difference [15].

In analogy with the Widom test-particle method [54], this implementation of the variational route is also called the test-area method [36, 55]. Following Sampayo *et al.* [22], it can be applied to curved interfaces, where the affine transformation scales one of the cartesian axes by the factor $1/(1+\xi)$ and the remaining ones by $(1+\xi)^{1/2}$. For $\xi > 0$, this creates an oblate shape and the area of the surface of tension is increased by [56]

$$\frac{\Delta a}{\pi R_\rho^2} = 2(1+\xi) + \frac{\ln([1+\Xi]/[1-\Xi])}{(1+\xi)^2\Xi} + \mathcal{O}\left(\frac{\delta\,\Delta a}{R_\rho^3}\right), \quad (24)$$

with the ellipticity of the average equimolar surface in the perturbed system given by $\Xi = [1-(1+\xi)^{-3}]^{1/2}$. In the prolate case ($\xi < 0$), the corresponding term is $\Xi = [1-(1-\xi)^{-3}]^{1/2}$ with [56]

$$\frac{\Delta a}{\pi R_\rho^2} = 2\left(\frac{\arcsin\Xi}{\Xi(1-\xi)^{1/2}} - \xi - 1\right) + \mathcal{O}\left(\frac{\delta\,\Delta a}{R_\rho^3}\right). \quad (25)$$

It can be shown that the first-order term in Eq. (23) is equivalent to the Kirkwood-Buff [57] mechanical route expression for the surface tension [58]. The higher-order terms therefore presumably capture the deviation between the mechanical and variational routes due to fluctuations or, equivalently, the contribution of non-equilibrium configurations to γ. Thus, the higher-order contribution to Eq. (23) may be related to the closed expression derived by Percus *et al.* [59] for the deviation between the actual free energy and an approximation based on the local pressure.

From this point of view, the following aspects of the method merit further consideration:

- While finite differences of higher order are taken into account for the energy, no such terms are considered for the surface area here. Clearly, the variance of ΔE is partly caused by the variance of Δa. The use of R_ρ for defining the surface area, cf. Eqs. (24) and (25), may lead to further deviations.

- The variance of ΔE accounts for surface oscillations such as long wave-length capillary waves, which directly relate to equilibrium properties of the interface and therefore do not depend on the statistical mechanical ensemble [39]. However, it can also be influenced by fluctuations regarding ρ' (at constant V') or V' (at constant ρ'). These modi are ensemble dependent, since they are coupled to the density of the vapour phase. Canonically, their amplitude increases with the total volume and is ill-defined in the thermodynamic limit $V \to \infty$. Therefore, the surface tension from the variational route may depend on the constraints imposed on the system by the ensemble.

- Although the volume associated with each of the phases is invariant for test-area transformations, there is still a distortion of the sample with respect to the equilibrium conformation. The method is therefore limited to isotropic phases, since shearing an anisotropic phase will induce an elastic contribution to ΔA from the bulk region as well.

III. DEVIATION OF THE EQUIMOLAR RADIUS FROM CAPILLARITY

From the Tolman equation in its approximate polynomial form, cf. Eq. (10), the excess equimolar radius η

can be related to the Tolman length δ by

$$\begin{aligned}\eta &= (\delta + R_\gamma) - R_\kappa \\ &= \delta + R_\gamma \left(1 - \left[1 + \frac{2\delta_0}{R_\gamma} + \mathcal{O}\big(R_\gamma^{-2}\big)\right]\right) \\ &= -\delta + \mathcal{O}\big(R_\gamma^{-1}\big),\end{aligned} \tag{26}$$

so that its magnitude in the zero-curvature limit is obtained as

$$\eta_0 = -\delta_0, \tag{27}$$

which is essentially equivalent to Eq. (13).

Both in the planar limit and in the presence of curvature effects, it is therefore possible to express the Tolman relations in terms of the easily accessible quantities η and φ, rather than δ and $1/R_\gamma$. The point of departure for such an expression is the exact closed form of the Tolman equation, cf. Eq. (9). It should be recalled that this expression is derived from the Gibbs-Duhem equation, the Young-Laplace equation and the Gibbs adsorption equation [17]; hence, it is based entirely on an axiomatic thermodynamic treatment. As opposed to truncated power series of the form of Eq. (10), the alternative description remains valid when the radius R_γ becomes similar or smaller in magnitude than the Tolman length. Polynomial expansions in terms of δ/R_γ necessarily fail to capture this limit.

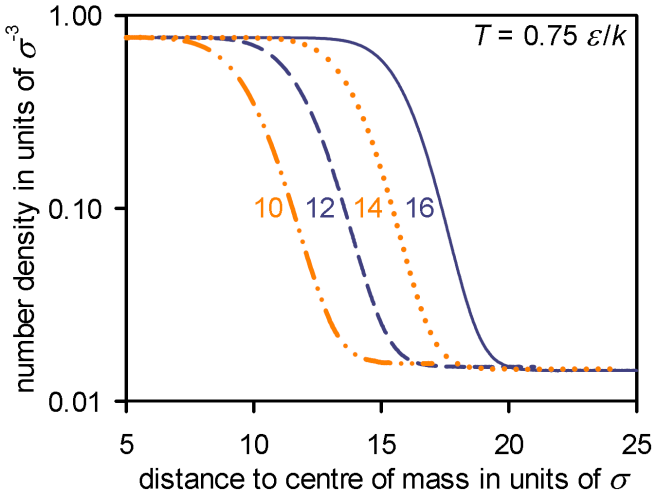

Figure 2. Density profiles from canonical MD simulations of LJTS liquid drops at $T = 0.75\ \varepsilon/k$ with equimolar radii of $R_\rho = 9.977 \pm 0.001$ ($\cdot$ — $\cdot$), 12.029 ± 0.003 (– –), $13.974 \pm 0.002\ \sigma$ ($\cdots$) and $15.967 \pm 0.001\ \sigma$ (—), cf. Tabs. I and II.

From the Young-Laplace equation, it follows that

$$\frac{dR_\gamma}{d\varphi} = \frac{1}{\varphi}\frac{d\gamma}{d\varphi} - \frac{\gamma}{\varphi^2}, \tag{28}$$

while the reduced length scale appearing in the Tolman equation can be transformed to

$$\frac{\delta}{R_\gamma} = \frac{\eta\varphi + \gamma_0}{\gamma} - 1, \tag{29}$$

by using Eqs. (1), (4), (8) and (11). The Tolman relation can thus be converted to

$$\frac{d\gamma}{d\varphi} = -\frac{2\gamma}{\varphi}\left(\frac{\delta}{R_\gamma} + \left[\frac{\delta}{R_\gamma}\right]^2 + \frac{1}{3}\left[\frac{\delta}{R_\gamma}\right]^3\right) \tag{30}$$

$$= \frac{2\gamma}{3\varphi}\left(1 - \left[\frac{\eta\varphi + \gamma_0}{\gamma}\right]^3\right). \tag{31}$$

This representation of the Tolman result is fully equivalent to Eq. (9).

For $\varphi \to 0$, further considerations are required. There, the curvature dependence of γ as specified by Eq. (31) is only self-consistent under an additional condition. To demonstrate this, it is helpful to consider the exact Tolman equation in a different form

$$\frac{d\gamma}{d\varphi} = \frac{2}{\gamma^2}\left(\frac{1}{3}\left[\zeta - \eta^3\varphi^2\right] - \gamma_0\eta[\gamma_0 + \eta\varphi]\right), \tag{32}$$

which follows from Eq. (31) by expanding the cubic term where ζ has been defined as

$$\zeta = \frac{\gamma^3 - \gamma_0^3}{\varphi}. \tag{33}$$

For the sake of brevity, the notation $q_i = \lim_{\varphi\to 0} d^i q/d\varphi^i$ is used here for the i-th derivative of a quantity q in the zero-curvature limit. The slope of γ can be obtained by inserting

$$\zeta_0 = \left(\gamma^3\right)_1 = 3\gamma_0^2\gamma_1, \tag{34}$$

into Eq. (32), which yields

$$\gamma_1 = 2\eta_0. \tag{35}$$

Expanding the excess equimolar radius as

$$\eta = \eta_0 + \eta_1\varphi + \mathcal{O}(\varphi^2), \tag{36}$$

and inserting this expression as well as Eq. (35) into the planar limit for Eq. (32) leads to

$$\left(\gamma^3\right)_2 = 12\gamma_0\eta_0^2, \tag{37}$$

and

$$\gamma_0\gamma_2 = -4\eta_0^2. \tag{38}$$

It is by considering the zero-curvature limit for the third derivative of γ^3 that a theorem for the slope of η can now be deduced. Based on Eqs. (34) and (37), a Taylor expansion for $d(\gamma^3)/d\varphi$ in terms of φ

$$\frac{d}{d\varphi}\gamma^3 = \left(\gamma^3\right)_1 + \left(\gamma^3\right)_2\varphi + \frac{1}{2}\left(\gamma^3\right)_3\varphi^2 + \mathcal{O}(\varphi^3), \tag{39}$$

yields

$$\begin{aligned}\zeta &= \frac{1}{\varphi}\int_0^\varphi d\varphi\left(\frac{d}{d\varphi}\gamma^3\right) \\ &= 6\gamma_0^2\eta_0 + 6\gamma_0\eta_0^2\varphi + \frac{\varphi^2}{6}\left(\gamma^3\right)_3 + \mathcal{O}(\varphi^3).\end{aligned} \tag{40}$$

From Eqs. (35) to (40)

$$6\gamma_0\left(\gamma_0\eta_1+\eta_0^2\right)+\frac{\varphi}{6}\left(\gamma^3\right)_3=0+\mathcal{O}(\varphi), \qquad (41)$$

follows by applying the full Tolman equation, cf. Eq. (32), in the planar limit. However, this implies

$$\eta_1=-\frac{\eta_0^2}{\gamma_0}, \qquad (42)$$

which constitutes a necessary boundary condition for the Tolman approach in terms of η and φ.

Thus, while there is a direct correspondence between δ_0 and η_0, no such relation exists in case of δ_1 and η_1, i.e., the respective derivatives (in terms of φ) in the zero-curvature limit; instead, η_1 is fully determined by η_0 and thus by δ_0, the Tolman length of the planar interface. This means that data on the excess equimolar radius for large radii have a double significance regarding the planar limit: on the one hand, they can be extrapolated to $\varphi = 0$, leading to an estimate for the planar Tolman length and the curvature dependence of γ to first order in terms of φ or $1/R_\gamma$; on the other hand, the slope of η is in itself relevant, since its zero-curvature limit η_1 also provides information on η_0.

The equivalent of the exact Tolman equation in terms of the excess equimolar radius η and the pressure difference characterized by φ is Eq. (31). An expansion as a power series, analogous to Eq. (10), can be expressed as

$$\gamma=\gamma_0+2\eta_0\varphi-\frac{2\eta_0^2}{\gamma_0}\varphi^2+\mathcal{O}(\varphi^3). \qquad (43)$$

The planar limit, where higher order terms can be neglected, can be treated accurately with expressions like Eq. (43). Away from the planar limit, Eq. (31) applies without any further condition (since the boundary condition for the slope of η is only relevant for $\varphi \to 0$), while Eq. (43) becomes an approximation.

IV. THE EXCESS EQUIMOLAR RADIUS FROM MOLECULAR SIMULATION

With the *mardyn* MD program, developed by Bernreuther and co-workers [60–62], the canonical ensemble was simulated for small systems, corresponding to equilibrium conditions for nanoscopic liquid drops surrounded by supersaturated vapours. The truncated-shifted Lennard-Jones (LJTS) pair potential

$$u(r)=\begin{cases}4\varepsilon\left[\left(\frac{\sigma}{r}\right)^{12}-\left(\frac{\sigma}{r}\right)^{6}\right]+u_{\text{shift}}, & \text{for } r<r_\text{c},\\ 0, & \text{for } r\geq r_\text{c},\end{cases} \qquad (44)$$

with the size parameter σ, the energy parameter ε and a cutoff at $r_\text{c} = 2.5\ \sigma$ is applied as a fluid model here, including a shift by $u_\text{shift} = 4\varepsilon\left[(\sigma/r_\text{c})^6-(\sigma/r_\text{c})^{12}\right]$ to make the potential continuous. The LJTS model is an adequate basis for investigating bulk and interfacial properties of simple spherical conformal fluids (e.g., noble gases and methane) on a molecular level, cf. Vrabec *et al.* [25]. On account of this, numerous studies on nanoscopic liquid drops have been reported [18, 24, 25, 63–67]. The LJTS fluid can thus be regarded as a key benchmark for theoretical and simulation approaches to the problem of curved vapour-liquid interfaces.

Certain of the general properties of this simple model, taking only short-range interactions into account, can be assumed to carry over to polar fluids as well [68], except for temperatures in the vicinity of the critical point. It is clear, however, that a qualitatively different behaviour should be expected for liquid drops formed by water with and without ionic species [69, 70], liquid crystals [71] and similar complex organic molecules. Such systems are beyond the scope of the present study.

Liquid drops are investigated at temperatures between $T = 0.65$ and $0.95\ \varepsilon/k$, covering most of the range between the triple point temperature (which is ≈ 0.55 according to Bolhuis and Chandler [72], ≈ 0.618 as determined by Toxværd [73] and $\approx 0.65\ \varepsilon/k$ according to van Meel *et al.* [65]) and the critical temperature which several independent studies have consistently obtained as $1.08\ \varepsilon/k$ for the LJTS fluid [25, 74, 75]. The Verlet leapfrog algorithm is employed to solve the classical equations of motion numerically with an integration time step of 0.002 in Lennard-Jones time units, i.e., $\sigma\sqrt{m/\varepsilon}$, where m is the mass of a particle. Cubic simulation volumes with 290 to 126 000 particles, applying the periodic boundary condition, are equilibrated for at least 2 000 time units. Subsequently, spherically averaged density profiles $\rho(z)$, with their origin ($z = 0$) at the centre of mass of the whole system, are constructed with a binning scheme based on equal volume concentrical spheres using sampling intervals between 1 000 and 40 000 time

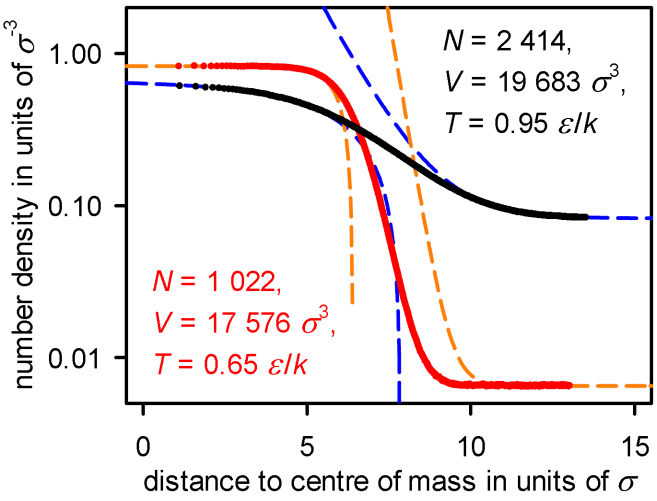

Figure 3. Density profiles from canonical MD simulations of LJTS liquid drops at $T = 0.65$ and $0.95\ \varepsilon/k$, showing the average densities from simulation (•) and exponential approximants (– –). The steeper profile corresponds to the lower temperature.

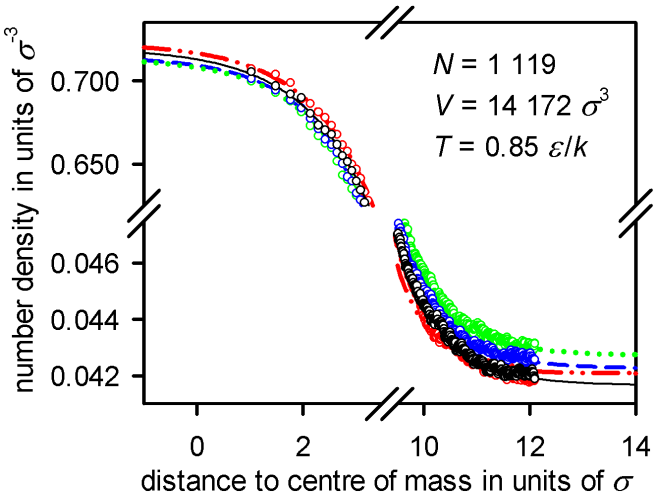

Figure 4. Density profiles from a single canonical MD simulation of a LJTS liquid drop at $T = 0.85\ \varepsilon/k$, showing the average densities from simulation (∘) and exponential approximants (lines) corresponding to the sampling intervals 2 000 – 3 000 (· · ·; green), 3 000 – 4 000 (· · · – · · ·; red), 4 000 – 5 000 (– –; blue) and 5 000 – 6 000 time units (—; black) after the onset of the simulation. The standard deviation between the densities at an infinite distance from the interface, according to the exponential fits for all sampling intervals of a single MD simulation, is used to determine the error of the bulk densities here.

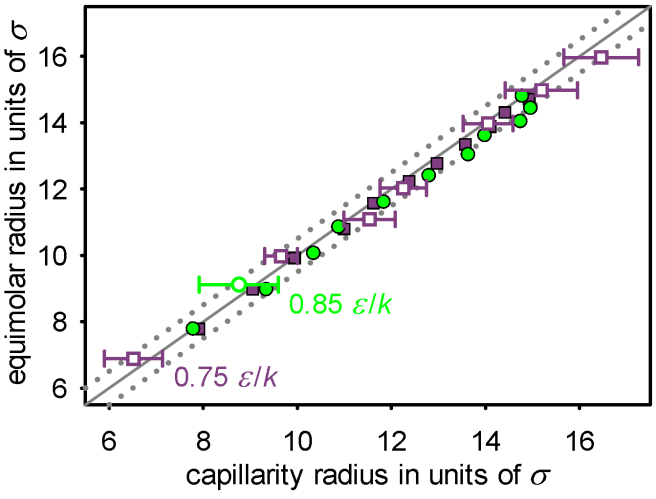

Figure 5. Equimolar radius R_ρ as a function of the capillarity radius R_κ for LJTS liquid drops, from density profiles and bulk pressures determined with canonical MD simulations at $T = 0.75$ (□) and $0.85\ \varepsilon/k$ (∘), in comparison with results from previous work of Vrabec *et al.* [25] at $T = 0.75$ (■) and $0.85\ \varepsilon/k$ (•), using pressure differences based on evaluating the IK tensor in the (approximately) homogeneous regions inside and outside the liquid drop. The continuous diagonal line is defined by $R_\rho = R_\kappa$ and thus corresponds to an excess equimolar radius of $\eta = 0$, while the dotted lines correspond to $\eta = \pm 0.5\ \sigma$.

units, depending on the (expected) total simulation time, to gather multiple samples for each system. Examples of the density profiles obtained according to this method are shown in Figs. 2 – 4.

The density profiles of LJTS vapour-liquid interfaces are known to agree well with an expression based on two hyperbolic tangent terms, to which $\rho(z)$ has been successfully correlated for liquid drops by Vrabec *et al.* [25]. The present method, however, merely requires the bulk densities ρ' and ρ'' corresponding to a certain value of μ or φ, which are determined here by correlating the outer part of the density profile and extrapolating it to regions far from the interface. The densities of the coexisting fluid phases are thus deduced from simulation results by correlating the exponential terms

$$\begin{aligned} \rho' &= \rho(z) + \alpha' \exp\left(\beta'[z - z']\right), \\ \rho'' &= \rho(z) - \alpha'' \exp\left(\beta''[z'' - z]\right), \end{aligned} \tag{45}$$

to the data for the inner- and outermost spherical bins of the density profiles, cf. Fig. 3. These terms, which are based on those employed by Lekner and Henderson [58], asymptotically agree with the hyperbolic tangent expression of Vrabec *et al.* [25]. From the liquid and vapour densities ρ' and ρ'' of the fit to Eq. (45), the equimolar radius R_ρ is calculated according to Eq. (2). The respective margins of error are obtained as standard deviations from the profiles belonging to different sampling intervals of the same MD simulation, cf. Fig. 4, of which there are at least three in all cases. The corresponding pressures p' and p'' are computed by canonical MD simulation of the bulk fluid at the respective densities.

For the surface tension in the zero-curvature limit, the values $\gamma_0(0.65\,\varepsilon/k) = 0.680 \pm 0.009$, $\gamma_0(0.75\,\varepsilon/k) = 0.493 \pm 0.008$, $\gamma_0(0.85\,\varepsilon/k) = 0.317 \pm 0.007$ and $\gamma_0(0.95\,\varepsilon/k) = 0.158 \pm 0.006\ \varepsilon\sigma^{-2}$ are taken from the correlation of Vrabec *et al.* [25]; the error corresponds to the individual data points for γ_0 from the same source. In case of $T = 0.9\ \varepsilon/k$, the higher precision of the computations of van Giessen and Blokhuis [24] is exploited, using the value $\gamma_0 = 0.227 \pm 0.002\ \varepsilon\sigma^{-2}$ obtained from a linear fit to data for the curved interface [24], cf. Fig. 1. The assumption made for the error is rather generous in this case, considering the even higher confidence suggested by the agreement between the individual data points for φR_ρ.

Combining these quantities leads to the capillarity radius R_κ and the excess equimolar radius η. Note that the margin of error for η, as indicated in Tab. I, contains contributions quantifying the accuracy of γ_0 and the precision of the MD simulations of the liquid drop itself as well as those of the homogeneous vapour and liquid phases. While the vapour pressure p'' and the equimolar radius R_ρ could be obtained with a high precision, the liquid pressure and the surface tension in the zero-curvature limit are major sources of uncertainty here. In both cases, methodical changes can be expected to increase the precision significantly: regarding γ_0, it can be seen from Fig. 1 that it is now possible to reach a level of confidence bey-

Table I. An analysis of the error of the excess equimolar radius η of LJTS liquid drops at the temperature $T = 0.75\ \varepsilon/k$. The number of particles N, the volume V of the periodic simulation box and the total simulation time t for the simulations of the liquid drops are indicated alongside the contributions to the uncertainty of η from the pressure p' of the liquid phase (determined by canonical MD simulation of the bulk liquid), the surface tension γ_0 of the planar vapour-liquid interface, cf. Vrabec et al. [25], the vapour pressure p'' (analogous to p') and the equimolar radius R_ρ (from the density profiles of the liquid drops). Note that the time unit, i.e., $\sigma\sqrt{m/\varepsilon}$, corresponds to 500 simulation time steps here. The flat symbols ($\flat$) indicate the fraction of the margin of error for η due to the respective quantities. All values are given in Lennard-Jones units, and the error in terms of the last digit is specified in parentheses. In the subsequent discussion, the cases where the uncertainty of η exceeds σ are disregarded.

N	$V\ [\sigma^{-3}]$	$t\ [\sigma\sqrt{m/\varepsilon}]$	$p'\ [\varepsilon\sigma^{-3}]$	$\flat\, p'$	$\flat\, \gamma_0$	$p''\ [\varepsilon\sigma^{-3}]$	$\flat\, p''$	$R_\rho\ [\sigma]$	$\flat\, R_\rho$	$\eta\ [\sigma]$
497	10 648	60 000	0.6(1)	84 %	5.9 %	0.0135(3)	0.23 %	4.33(5)	9.5 %	2.5(5)
1 418	21 952	48 176	0.16(1)	82 %	17 %	0.01136(5)	0.37 %	6.883(3)	0.5 %	0.4(6)
1 766	21 952	6 000	0.14(3)	94 %	5.3 %	0.0110(2)	0.58 %	7.61(1)	0.55 %	0(2)
3 762	39 304	221 244	0.113(2)	53 %	45 %	0.01042(4)	1.0 %	9.977(1)	0.28 %	0.3(3)
5 161	54 872	64 219	0.096(3)	63 %	34 %	0.0104(1)	2.4 %	11.089(4)	0.82 %	−0.4(5)
6 619	74 088	162 678	0.090(2)	59 %	40 %	0.01007(2)	0.75 %	12.029(3)	0.57 %	−0.2(5)
10 241	110 592	185 460	0.080(1)	56 %	43 %	0.00985(2)	0.58 %	13.974(2)	0.29 %	−0.1(5)
12 651	140 608	32 594	0.075(2)	66 %	32 %	0.00974(4)	1.2 %	14.981(6)	0.78 %	−0.2(8)
15 237	166 375	135 348	0.070(2)	66 %	33 %	0.00969(1)	0.35 %	15.967(1)	0.15 %	−0.5(8)
17 113	169 418	6 006	0.08(1)	89 %	9.8 %	0.00969(9)	0.78 %	16.689(4)	0.18 %	2(2)
24 886	238 328	27 272	0.069(9)	90 %	9.7 %	0.00947(3)	0.3 %	18.969(5)	0.17 %	2(3)
28 327	238 328	6 006	0.056(9)	92 %	7.5 %	0.00945(3)	0.28 %	19.950(8)	0.18 %	−1(5)
38 753	247 673	6 000	0.050(7)	90 %	8.8 %	0.00932(5)	0.69 %	22.391(7)	0.15 %	−2(4)
125 552	697 078	6 006	0.042(5)	89 %	9.6 %	0.00908(9)	1.6 %	33.31(1)	0.21 %	3(5)

Table II. Number of particles N, volume V of the periodic simulation box and temperature T of the present canonical ensemble MD simulations of the LJTS fluid and equilibrium properties of the liquid drop as well as the surrounding vapour, i.e., the respective densities ρ', ρ'' and pressures p', p'' as well as the capillarity radius R_κ, the equimolar radius R_ρ and the excess equimolar radius η. For drop radii above 8 σ, these values can be reliably regarded as identical with those corresponding to the present theoretical approach, which is highlighted with the bold typeface. In case of smaller radii (cursive typeface), inaccuracies can arise due to the application of exponential approximants, cf. Fig. 3 and Eq. (45), so that the respective values can, at present, be acknowledged as phenomenological quantities only. All values are given in Lennard-Jones units, and the error in terms of the last digit is specified in parentheses.

N	$V\ [\sigma^3]$	$T\ [\varepsilon/k]$	$\rho'\ [\sigma^{-3}]$	$\rho''\ [\sigma^{-3}]$	$p'\ [\varepsilon\sigma^{-3}]$	$p''\ [\varepsilon\sigma^{-3}]$	$R_\kappa\ [\sigma]$	$R_\rho\ [\sigma]$	$\eta\ [\sigma]$
291	8 999	0.65	*0.857(5)*	*0.0090(2)*	*0.65(8)*	*0.0054(1)*	*2.1(3)*	*3.90(1)*	*1.8(3)*
1 022	17 576	0.65	*0.830(1)*	*0.00651(7)*	*0.22(2)*	*0.00397(4)*	*6.3(6)*	*6.407(2)*	*0.1(6)*
497	10 648	0.75	*0.81(1)*	*0.0214(6)*	*0.6(1)*	*0.0135(4)*	*1.8(5)*	*4.33(5)*	*2.5(5)*
1 418	21 952	0.75	*0.777(1)*	*0.0173(1)*	*0.16(1)*	*0.01136(5)*	*6.5(6)*	*6.883(3)*	*0.4(6)*
3 762	39 304	0.75	**0.7721(2)**	**0.01566(6)**	**0.113(2)**	**0.01042(4)**	**9.7(4)**	**9.977(1)**	**0.3(4)**
5 161	54 872	0.75	**0.7703(2)**	**0.0156(2)**	**0.096(3)**	**0.0104(1)**	**11.5(5)**	**11.089(4)**	**−0.5(6)**
6 619	74 088	0.75	**0.7697(2)**	**0.01506(4)**	**0.091(2)**	**0.01007(2)**	**12.3(5)**	**12.029(3)**	**−0.2(5)**
10 241	110 592	0.75	**0.7685(1)**	**0.01469(3)**	**0.080(2)**	**0.00985(2)**	**14.1(5)**	**13.974(2)**	**−0.1(5)**
12 651	140 608	0.75	**0.7679(2)**	**0.01451(7)**	**0.075(2)**	**0.00974(4)**	**15.2(8)**	**14.981(6)**	**−0.2(8)**
15 237	166 375	0.75	**0.7673(2)**	**0.01442(2)**	**0.070(2)**	**0.00969(1)**	**16.5(8)**	**15.967(1)**	**−0.5(8)**
1 119	14 172	0.85	*0.733(7)*	*0.0421(5)*	*0.23(5)*	*0.0273(2)*	*3.1(9)*	*6.79(6)*	*2.5(9)*
3 357	32 768	0.85	**0.7135(8)**	**0.0371(5)**	**0.097(5)**	**0.0249(2)**	**8.8(8)**	**9.11(1)**	**0.4(9)**
2 031	21 952	0.9	*0.687(3)*	*0.0573(8)*	*0.13(1)*	*0.0369(3)*	*5.1(8)*	*6.79(6)*	*1.7(9)*
4 273	29 791	0.9	**0.6773(9)**	**0.0532(2)**	**0.082(4)**	**0.03516(7)**	**9.7(9)**	**10.086(9)**	**0.4(9)**
11 548	85 184	0.9	**0.6738(1)**	**0.0504(2)**	**0.0672(6)**	**0.03396(8)**	**13.7(4)**	**14.054(8)**	**0.4(4)**
2 414	19 683	0.95	*0.662(2)*	*0.0825(2)*	*0.169(7)*	*0.05032(8)*	*2.7(3)*	*6.86(3)*	*4.2(3)*

ond that of the data of Vrabec *et al.* [25] which are also used here. For the pressure of the liquid p', approaches based on the chemical potential, which can be determined in any region of the simulation volume (including the vapour phase), can be expected to lead to significant improvements in combination with a reliable equation of state or high-precision simulations in the grand canonical ensemble.

A full summary of the simulation results where η could be determined with error bars smaller than σ is given in Tab. II. Note that to achieve full consistency with the Tolman approach, the bulk densities ρ' and ρ'' from Eq. (45) have to match those of the bulk fluid at the same temperature and chemical potential as the two-phase system. Regarding liquid drops with $R_\rho > 8\ \sigma$, this is certainly the case, since constant density regions coexisting with the interface are actually present, cf. Fig. 2. However, the values determined for the smallest drops here rely on the validity of the correlation given by Eq. (45) and can be considered valid only as far as this expression itself does not introduce any major deviations, an assertion that remains open to further examination; a version of the present method computing p' via μ could resolve this issue.

V. DISCUSSION

Previous authors have made qualitatively contradictory claims on the magnitude of the Tolman length as well as its sign: Tolman himself expected δ to be positive and smaller than the length scale of the dispersive interaction, a conjecture that Kirkwood and Buff [57] affirmed from a statistical mechanical point of view, based on a mechanical approach. Subsequent studies, however, have also found δ to be negligible or even equal to zero [20, 63, 76], positive and larger than σ [25, 66], negative with $-\sigma < \delta < 0$ [22, 24, 77] or negative and diverging ($\delta_0 = -\infty$) in the planar limit [78], while others have claimed that the sign of δ is curvature dependent itself [79, 80]. Thereby, they have only proven the mutual inconsistency of their assumptions and methods, while nothing is truely known about δ and the dependence of the surface tension on curvature.

The new approach introduced in Section III is strictly based on axiomatic thermodynamics and relies on the fact that $\delta_0 = -\eta_0$ holds in the planar limit. From the values for η reported in bold face in Tab. II, corresponding to $R_\rho > 8\ \sigma$, the excess equimolar radius for liquid drops of the LJTS fluid is unequivocally shown to be smaller in magnitude than $\sigma/2$, while its remains unclear whether it is positive, negative, of both signs (depending on the curvature) or equal to zero. Since this means that at the present level of accuracy, no significant dependence of γ on the radius of the liquid drop could be detected, the statement of Mareschal *et al.* [81] regarding cylindrical interfaces also applies here: considering «the large fluctuations in the bulk liquid phase», cf. the error analysis presented in Tab. I, «we tentatively conclude that the surface tension is independent of the curvature of the liquid-vapor interface or else that this dependence is very weak.»

The only view that can be definitely dismissed is that of a large and positive Tolman length, previously held by some of the present authors on the basis of results from the mechanical route to the surface tension, employing the IK pressure tensor [25, 66]. As Fig. 5 shows, the previous simulation results are actually consistent with those from the present study if they are interpreted in terms of the radii R_κ and R_ρ. Thereby, following the approach of van Giessen and Blokhuis [24], only the density profile and the pressure in the homogeneous regions inside and outside the liquid drop are taken into account, whereas the normal pressure along the interface is not considered at all. Since the deviation between present and previous data disappears in such a representation, the disagreement must be caused by the inadequacy of the pressure-tensor (mechanical) route implemented by Thompson *et al.* [34], as pointed out by Henderson [39, 82]. Possible sources of error for this approach are outlined in Section II. Nonetheless, more detailed methodological investigations are expedient to determine which approximations are actually responsible for major inaccuracies, and whether they can be corrected or whether the pressure-tensor route to the surface tension has to be discarded altogether.

ACKNOWLEDGMENTS

The present work contributes to the IMEMO project of the German Federal Ministry of Education and Research (BMBF) and to the Collaborative Research Centre (SFB) 926 of the German Research Foundation (DFG). It was conducted under the auspices of the Boltzmann-Zuse Society of Compuational Molecular Engineering (BZS). The position of M. T. Horsch at Imperial College London was funded by a fellowship within the postdoc programme of the German Academic Exchange Service (DAAD), and G. Jackson as well as E. A. Müller are grateful to the Engineering and Physical Sciences Research Council (EPSRC) of the UK (grants GR/T17595, GR/N35991 and EP/E016340), the Joint Research Equipment Initiative (GR/M94427), and the Royal Society-Wolfson Foundation refurbishment scheme for additional funding to the Molecular Systems Engineering Group. The computations were performed on the NEC Nehalem cluster *laki* at the High Performance Computing Center Stuttgart (HLRS) with resources allocated according to the grant MMHBF. At the HLRS, the authors would like to thank M. F. Bernreuther for his support in general and for coordinating the MMHBF grant as well as the development of the MD code *mardyn*. Furthermore, D. Reguera López and J. Wedekind (Barcelona), F. Römer (London), M. Schrader (Mainz), Z. Lin, S. K. Miroshnichenko, S. Olma, Z. Wei (Paderborn) and D. V. Tatyanenko (St. Peters-

burg) as well as S. Dietrich, S. Grottel, C. Niethammer and G. Reina (Stuttgart) are acknowledged for contributing to various theoretical and practical issues through helpful suggestions and their participation in relevant discussions or by assisting at the debugging process.

[1] T. Young, Phil. Trans. R. Soc. Lond. **95**, 65 (1805).
[2] P.-S. de Laplace, *Traité de méchanique céleste*, vol. 3 (Bachelier, Paris, 1806).
[3] J. S. Rowlinson and B. Widom, *Molecular Theory of Capillarity* (Clarendon Press, Oxford, 1982), ISBN 0-486-42544-4.
[4] J. W. Gibbs, Transact. Connecticut Acad. Arts Sci. **3**, 108 (1878).
[5] J. W. Gibbs, Am. J. Sci. (ser. 3) **16**, 441 (1878).
[6] M. Volmer and A. Weber, Z. phys. Chem. **119**, 277 (1926).
[7] L. Farkas, Z. phys. Chem. **125**, 236 (1927).
[8] R. Becker and W. Döring, Ann. Phys. **24**, 719 (1935).
[9] F. Kuhrt, Z. Phys. **131**, 185 (1952).
[10] J. Feder, K. C. Russell, J. Lothe and G. M. Pound, Adv. Phys. **15**, 111 (1966).
[11] R. H. Weber, Ann. Phys. **4**, 706 (1901).
[12] F. P. Buff, J. Chem. Phys. **19**, 1591 (1951).
[13] F. P. Buff, J. Chem. Phys. **23**, 419 (1955).
[14] S. Kondo, J. Chem. Phys. **25**, 662 (1956).
[15] R. C. Tolman, J. Chem. Phys. **16**, 758 (1948).
[16] R. C. Tolman, J. Chem. Phys. **17**, 118 (1949).
[17] R. C. Tolman, J. Chem. Phys. **17**, 333 (1949).
[18] B. J. Block, S. K. Das, M. Oettel, P. Virnau and K. Binder, J. Chem. Phys. **133**, 154702 (2010).
[19] A. J. Castellanos Suárez, J. Toro Mendoza and M. García Sucre, J. Phys. Chem. B **133**, 5981 (2009).
[20] T. Bieker and S. Dietrich, Physica A **252**, 85 (1998), Physica A **259**, 466 (1998).
[21] M. Schrader, P. Virnau, D. Winter, T. Zykova-Timan and K. Binder, Eur. Phys. J. Spec. Top. **177**, 103 (2009).
[22] J. G. Sampayo, A. Malijevský, E. A. Müller, E. de Miguel and G. Jackson, J. Chem. Phys. **132**, 141101 (2010).
[23] M. J. P. Nijmeijer, C. Bruin, A. B. van Woerkom, A. F. Bakker and J. M. J. van Leeuwen, J. Chem. Phys. **96**, 565 (1991).
[24] A. E. van Giessen and E. M. Blokhuis, J. Chem. Phys. **131**, 164705 (2009).
[25] J. Vrabec, G. K. Kedia, G. Fuchs and H. Hasse, Mol. Phys. **104**, 1509 (2006).
[26] P. R. ten Wolde and D. Frenkel, J. Chem. Phys. **109**, 9901 (1998).
[27] H. Matsubara, T. Koishi, T. Ebisuzaki and K. Yasuoka, J. Chem. Phys. **127**, 214507 (2007).
[28] J. Vrabec, M. Horsch and H. Hasse, J. Heat Transfer **131**, 043202 (2009).
[29] Z.-Y. Hou, L.-X. Liu, R.-S. Liu, Z.-A. Tian and J.-G. Wang, Chem. Phys. Lett. **491**, 172 (2010).
[30] G. Chkonia, J. Wölk, R. Strey, J. Wedekind and D. Reguera, J. Chem. Phys. **130**, 064505 (2009).
[31] M. P. A. Fisher and M. Wortis, Phys. Rev. B **29**, 6252 (1984).
[32] E. M. Blokhuis and D. Bedeaux, Mol. Phys. **80**, 705 (1993).
[33] T. V. Bykov and A. K. Shchekin, Inorganic Materials **35**, 641 (1999).
[34] S. M. Thompson, K. E. Gubbins, J. P. R. B. Walton, R. A. R. Chantry and J. S. Rowlinson, J. Chem. Phys. **81**, 530 (1984).
[35] M. Schrader, P. Virnau and K. Binder, Phys. Rev. E **79**, 061104 (2009).
[36] G. J. Gloor, G. Jackson, F. J. Blas and E. de Miguel, J. Chem. Phys. **123**, 134703 (2005).
[37] A. Ghoufi, F. Goujon, V. Lachet and P. Malfreyt, Phys. Rev. E **77**, 031601 (2008).
[38] A. Ghoufi and P. Malfreyt, J. Chem. Phys. (2011), submitted.
[39] J. R. Henderson, in *Fluid Interfacial Phenomena*, edited by C. A. Croxton (Wiley, New York, 1986), pp. 555–605, ISBN 0-471-90757-X.
[40] G. Bakker, *Kapillarität und Oberflächenspannung*, no. 6 in Handbuch der Experimentalphysik (Akademische Verlagsgesellschaft, Leipzig, 1928).
[41] A. Harasima, J. Phys. Soc. Jpn. **8**, 343 (1953).
[42] V. G. Baidakov and G. S. Boltachev, Phys. Rev. E **59**, 469 (1999).
[43] J. H. Irving and J. G. Kirkwood, J. Chem. Phys. **18**, 817 (1950).
[44] J. R. Henderson and J. Lekner, Mol. Phys. **36**, 781 (1978).
[45] K. Binder, Phys. Rev. A **25**, 1699 (1982).
[46] J. P. R. B. Walton, D. J. Tildesley, J. S. Rowlinson and J. R. Henderson, Mol. Phys. **48**, 1357 (1983).
[47] P. Schofield and J. R. Henderson, Proc. Roy. Soc. A **379**, 231 (1982).
[48] G. M. Torrie and J. P. Valleau, J. Comp. Phys. **23**, 187 (1977).
[49] P. Virnau and M. Müller, J. Chem. Phys. **120**, 10925 (2004).
[50] M. J. McGrath, J. N. Ghogomu, N. T. Tsona, J. I. Siepmann, B. Chen, I. Napari and H. Vehkamäki, J. Chem. Phys. **133**, 084106 (2010).
[51] R. B. Nellas, S. J. Keasler, J. I. Siepmann and B. Chen, J. Chem. Phys. **132**, 164517 (2010).
[52] C. H. Bennett, J. Comp. Phys. **22**, 245 (1976).
[53] R. W. Zwanzig, J. Chem. Phys. **22**, 1420 (1954).
[54] B. Widom, J. Chem. Phys. **39**, 2808 (1963).
[55] F. J. Blas, L. G. MacDowell, E. de Miguel and G. Jackson, J. Chem. Phys. **129**, 144703 (2008).
[56] J. G. Sampayo Hernández, Ph.D. thesis (2010), Imperial College London.
[57] J. G. Kirkwood and F. P. Buff, J. Chem. Phys. **17**, 338 (1949).
[58] J. Lekner and J. R. Henderson, Mol. Phys. **34**, 333 (1977).
[59] J. K. Percus, L. A. Pozhar and K. E. Gubbins, Phys. Rev. E **51**, 261 (1995).
[60] M. Bernreuther and J. Vrabec, in *High Performance Computing on Vector Systems*, edited by M. Resch, T. Bönisch, K. Benkert, T. Furui and W. Bez (Springer, Heidelberg, 2006), pp. 187–195, ISBN 3-540-29124-5.
[61] M. Bernreuther, C. Niethammer, M. Horsch, J. Vrabec,

S. Deublein, H. Hasse and M. Buchholz, Innovatives Supercomputing in Deutschland **7**, 50 (2009).
[62] M. Buchholz, H.-J. Bungartz and J. Vrabec, J. Computational Sci. **2**, 124 (2011).
[63] Y. A. Lei, T. Bykov, S. Yoo and X. C. Zeng, J. Am. Chem. Soc. **127**, 15346 (2005).
[64] R. Hołyst and M. Litniewski, Phys. Rev. Lett. **100**, 055701 (2008).
[65] J. A. van Meel, A. J. Page, R. P. Sear and D. Frenkel, J. Chem. Phys. **129**, 204505 (2008).
[66] M. Horsch, J. Vrabec and H. Hasse, Phys. Rev. E **78**, 011603 (2008).
[67] I. Napari, J. Julin and H. Vehkamäki, J. Chem. Phys. **133**, 154503 (2010).
[68] I. Nezbeda, Mol. Phys. **103**, 59 (2005).
[69] R. G. Harrison and M. H. P. Ambaum, Proc. Roy. Soc. A **464**, 2561 (2008).
[70] N. Galamba, J. Chem. Phys. **133**, 124510 (2010).
[71] M. Houssa, L. F. Rull and J. M. Romero Enrique, J. Chem. Phys. **130**, 154504 (2009).
[72] P. G. Bolhuis and D. Chandler, J. Chem. Phys. **113**, 8154 (2000).
[73] S. Toxværd, J. Phys. Chem. C **111**, 15620 (2007).
[74] W. Shi and J. K. Johnson, Fluid Phase Equilib. **187–188**, 171 (2001).
[75] B. Smit, J. Chem. Phys. **96**, 8639 (2002).
[76] D. Zhou, M. Zeng, J. Mi and C. Zhong, J. Phys. Chem. B **115**, 57 (2011).
[77] S. J. Hemingway, J. R. Henderson and J. S. Rowlinson, Faraday Symp. Chem. Soc. **16**, 33 (1981).
[78] P. Bryk, R. Roth, K. R. Mecke and S. Dietrich, Phys. Rev. E **68**, 031602 (2003).
[79] K. Koga, X. C. Zeng and A. K. Shchekin, J. Chem. Phys. **109**, 4063 (1998).
[80] J. Julin, I. Napari, J. Merikanto and H. Vehkamäki, J. Chem. Phys. **133**, 044704 (2010).
[81] M. Mareschal, M. Baus and R. Lovett, J. Chem. Phys. **106**, 645 (1997).
[82] J. R. Henderson, J. Phys. Cond. Mat. **11**, 629 (1999).